UCLA
UCLA Previously Published Works

Title
Lipid-Bicelle-Coated Microfluidics for Intracellular Delivery with Reduced Fouling

Permalink
https://escholarship.org/uc/item/9h94772p

Journal
ACS Applied Materials & Interfaces, 12(41)

ISSN
1944-8244

Authors
Belling, Jason N
Heidenreich, Liv K
Park, Jae Hyeon
et al.

Publication Date
2020-10-14

DOI
10.1021/acsami.0c11485

Peer reviewed

eScholarship.org Powered by the California Digital Library
University of California

Author Manuscript

Author Manuscript

Author Manuscript

Author Manuscript

HHS Public Access

Author manuscript

ACS Appl Mater Interfaces. Author manuscript; available in PMC 2021 June 09.

Published in final edited form as:

ACS Appl Mater Interfaces. 2020 October 14; 12(41): 45744–45752. doi:10.1021/acsami.0c11485.

Lipid-Bicelle-Coated Microfluidics for Intracellular Delivery with Reduced Fouling

Jason N. Belling, **Liv K. Heidenreich**, **Jae Hyeon Park**, **Lisa M. Kawakami**, **Jack Takahashi**
California NanoSystems Institute and Department of Chemistry and Biochemistry, University of California, Los Angeles, Los Angeles, California 90095, United States

Isaura M. Frost
California NanoSystems Institute, Department of Pediatrics, David Geffen School of Medicine, and Department of Bioengineering, University of California, Los Angeles, Los Angeles, California 90095, United States;

Yao Gong, **Thomas D. Young**
California NanoSystems Institute and Department of Chemistry and Biochemistry, University of California, Los Angeles, Los Angeles, California 90095, United States

Joshua A. Jackman,
School of Chemical Engineering and SKKU-UCLA-NTU Precision Biology Research Center, Sungkyunkwan University, Suwon 16419, Republic of Korea;

Steven J. Jonas,
Department of Pediatrics, David Geffen School of Medicine, Children's Discovery and Innovation Institute, and Eli & Edythe Broad Center of Regenerative Medicine and Stem Cell Research, California NanoSystems Institute, University of California, Los Angeles, Los Angeles, California 90095, United States;

Nam-Joon Cho,
SKKU-UCLA-NTU Precision Biology Research Center, Sungkyunkwan University, Suwon 16419, Republic of Korea; School of Materials Science and Engineering, Nanyang Technological University, Singapore 639798 Singapore

Paul S. Weiss

Corresponding Authors: Steven J. Jonas – *Department of Pediatrics, David Geffen School of Medicine, Children's Discovery and Innovation Institute, and Eli & Edythe Broad Center of Regenerative Medicine and Stem Cell Research, California NanoSystems Institute, University of California, Los Angeles, Los Angeles, California 90095, United States*; sjonas@ucla.edu, **Nam-Joon Cho** – *SKKU-UCLA-NTU Precision Biology Research Center, Sungkyunkwan University, Suwon 16419, Republic of Korea; School of Materials Science and Engineering, Nanyang Technological University, Singapore 639798 Singapore*; njcho@ntu.edu.sg, **Paul S. Weiss** – *California NanoSystems Institute, Department of Chemistry and Biochemistry, Department of Bioengineering, and Department of Materials Science and Engineering, University of California, Los Angeles, Los Angeles, California 90095, United States; SKKU-UCLA-NTU Precision Biology Research Center, Sungkyunkwan University, Suwon 16419, Republic of Korea;* psw@cnsi.ucla.edu.

Supporting Information

The Supporting Information is available free of charge at https://pubs.acs.org/doi/10.1021/acsami.0c11485.
Additional cell viability and delivery efficiency data for bare and coated channels (PDF)

Complete contact information is available at: https://pubs.acs.org/10.1021/acsami.0c11485

The authors declare the following competing financial interest(s): P.S.W., S.J.J., N.-J.C., J.A.J., and J.N.B. are inventors on patent applications filed by the Regents of the University of California relating to the lipid-coated intracellular delivery platform.

Author Manuscript Author Manuscript Author Manuscript Author Manuscript

California NanoSystems Institute, Department of Chemistry and Biochemistry, Department of Bioengineering, and Department of Materials Science and Engineering, University of California, Los Angeles, Los Angeles, California 90095, United States; SKKU-UCLA-NTU Precision Biology Research Center, Sungkyunkwan University, Suwon 16419, Republic of Korea

Abstract

Innovative technologies for intracellular delivery are ushering in a new era for gene editing, enabling the utilization of a patient's own cells for stem cell and immunotherapies. In particular, cell-squeezing platforms provide unconventional forms of intracellular delivery, deforming cells through microfluidic constrictions to generate transient pores and to enable effective diffusion of biomolecular cargo. While these devices are promising gene-editing platforms, they require frequent maintenance due to the accumulation of cellular debris, limiting their potential for reaching the throughputs necessary for scalable cellular therapies. As these cell-squeezing technologies are improved, there is a need to develop next-generation platforms with higher throughput and longer lifespan, importantly, avoiding the buildup of cell debris and thus channel clogging. Here, we report a versatile strategy to coat the channels of microfluidic devices with lipid bilayers based on noncovalent lipid bicelle technology, which led to substantial improvements in reducing cell adhesion and protein adsorption. The antifouling properties of the lipid bilayer coating were evaluated, including membrane uniformity, passivation against nonspecific protein adsorption, and inhibition of cell attachment against multiple cell types. This surface functionalization approach was applied to coat constricted microfluidic channels for the intracellular delivery of fluorescently labeled dextran and plasmid DNA, demonstrating significant reductions in the accumulation of cell debris. Taken together, our work demonstrates that lipid bicelles are a useful tool to fabricate antifouling lipid bilayer coatings in cell-squeezing devices, resulting in reduced nonspecific fouling and cell clogging to improve performance.

Graphical Abstract

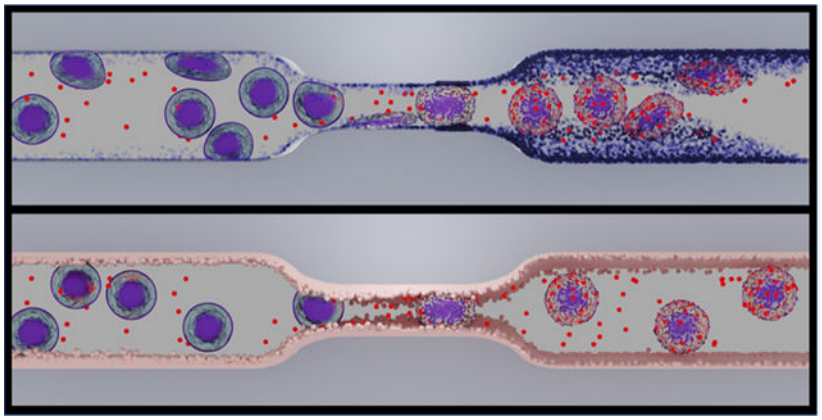

Keywords

bicelle; supported lipid bilayer; fouling; intracellular delivery; cell squeezing; microfluidics

Author Manuscript Author Manuscript Author Manuscript Author Manuscript

INTRODUCTION

Nonviral cell transfection technologies are promising for gene-delivery applications, as they have the potential to overcome the safety and technical limitations of viral vectors.[1] Among the variety of approaches that have been developed (e.g., electroporation, sonoporation, etc.), high-throughput platforms that physically squeeze cells have been popularized as noninvasive gene-editing approaches.[2–4] Sharei et al. demonstrated that transfection can occur when the cell diameter is larger than the microfluidic channel width, resulting in transient pores in the membrane.[5] This mechanism was used to deliver a variety of target molecules including DNA, RNA, and carbon nanotubes. This cell-squeezing microfluidic device has been able to transfect approximately 20,000 cells/s and is able to output ca. 1 million cells before clogging (where cells that adhere to the sidewalls prevent flow through the channel). To address this issue, more channels were added in parallel to increase throughput.[5] Another variant of cell squeezing used a combination of both physical and electrical permeabilization to promote diffusion of plasmids into cells while increasing viability by using a faster flow rate. In this work, Ding et al. found that combining these two techniques enabled a greater degree of transfection and increased the amount and type of cargo that could be introduced into mammalian cells.[6] Other researchers have utilized various geometries to deliver plasmids and large polysaccharides and achieved similar transfection performance.[7,8] Alternative methods that utilize hydroporation or acoustic pressure to form pores in the cell membrane have also been found to be effective intracellular delivery platforms.[9–11] Additional studies of these physical transfection devices have shown their utility for studying membrane repair and for gene-editing and therapeutic applications.[12–15] Although there have been dramatic improvements in the permeabilization of cellular membranes with physical methods, most microfluidic designs remain limited by the fouling of the channel walls by cells and their secreted proteins. This fouling is due to the hydrophobicity of the channel materials that are typically combinations of polydimethylsiloxane (PDMS) and glass/silica, which are inexpensive and straightforward to fabricate with micron-scale features using lithography.[16,17] As such, the development of surface coatings that are biomimetic and prevent nonspecific adsorption of cells would increase microfluidic channel lifetime and throughput, independent of the application. A passivating layer would also increase the fraction of the biomolecules delivered to cells instead of being adsorbed on the PDMS, improving control of the concentrations and delivery of biomolecular payloads.[18]

Indeed, a variety of approaches has been used to prevent nonspecific cell fouling in PDMS microchannels. An intuitive strategy is to examine the steric constraints on the system. For example, a “ratchet geometry” in the microfluidic channel can generate an oscillatory flow to sort and to separate circulating tumor cells according to their different deformability with clogging occurring only when the device volume is filled.[19] A more common method is to use poly(ethylene glycol) polymer coatings to prevent fouling on PDMS and glass surfaces.[20] Others have used surfactant treatments, such as Pluronic F68, to prevent protein adsorption and fibroblast adhesion to PDMS surfaces.[17] Self-assembled monolayers (SAMs) of siloxanes have also been used for preventing surface interactions between cells and proteins inside microfluidics. However, siloxane-based SAMs are difficult to characterize

Author Manuscript Author Manuscript Author Manuscript Author Manuscript

inside microfluidic channels due to the indirect methods required to assess SAM uniformity, such as measuring functionalized flat substrates and extrapolating the coating thickness and uniformity to the interior of the channels.[21] Therefore, designing a system that enables *direct* characterization of the channel walls would be advantageous for engineering the physicochemical properties of uniform channel coatings.

Lipids can be coupled with fluorophores, have lateral mobility when configured into bilayer assemblies, and have controllable compositions that can be tailored to have a wide range of electrostatic or chemical interactions.[22–25] Exploiting these properties, the uniformity of supported lipid bilayers can be characterized using fluorescence microscopy and can be prepared simply with lipid bicelles as precursors. In a previous work, coating channels with lipid bilayers increased resistance to antibody and protein adsorption by two orders of magnitude compared to those with bare surfaces, with the bilayers being stable for several weeks.[26,27] Other strategies for coatings include bovine serum albumin (BSA) passivation since BSA is known to prevent nonspecific protein adsorption to surfaces. Chiu et al. utilized the non-adhesive nature of BSA coatings to make confluent patterns of cells in microfluidic channels.[28] It was also demonstrated that cells do not adhere to bilayers in BSA-containing media.[29] However, the use of animal serum can stimulate fibronectin and vitronectin binding, resulting in integrin-dependent cell adhesion.[30] Supported lipid membranes can be designed to have protein-rich environments to mimic the rigidity of the extracellular matrix and can be used as effective cell-culture platforms.[31,32] In applications where whole blood or protein-containing serum is needed, there may be nonspecific binding events that occur with the fabricated lipid membranes. Nevertheless, Persson et al. demonstrated that lipid bilayer coatings in nanofluidic channels outperformed BSA passivation in preventing interactions between streptavidin-coated quantum dots, RecA proteins, and RecA-DNA complexes.[33] Groves et al. found that phospholipid bilayers patterned in corrals had no adhesion to HeLa cells except for lipid membranes containing phosphatidylserine.[34] Andersson et al. followed this work and showed supported lipid bilayers to be effective in preventing cell adhesion on SiO_2 and glass, even in protein-rich environments using egg yolk phosphatidylcholine.[35] Since phospholipid bilayers formed on solid supports prevent nonspecific protein and cell adhesion have direct methods of characterization and are naturally occurring in biological membranes, these molecules are excellent candidates for developing biomimetic engineering strategies to suppress cellular interactions with channel surfaces.

Here, we demonstrate a simple and scalable method to reduce nonspecific fouling and cell clogging in cell-squeeze devices by coating the microfluidic channel walls with lipid bicelles that spontaneously transform into a conformal supported lipid bilayer coating with high antifouling performance. Compared to other possible types of lipid nanostructures that can be used for lipid bilayer fabrication, bicelles are noteworthy because they readily form supported lipid bilayers under a wide range of conditions and are easily prepared with simple preparation processes and without stringent nanostructure size requirements. This coating strategy was applied to microchannels with cell squeeze constrictions, which significantly reduced the accumulation of cell debris in the channels. We further tested the intracellular delivery performance of these coated microfluidic constrictions using 40 kDa fluorescently labeled dextran and an enhanced green fluorescent protein-expressing plasmid

Author Manuscript Author Manuscript Author Manuscript Author Manuscript

(eGFP) and observed successful intracellular delivery and protein expression with viability exceeding 70% for all samples. Taken together, this passivation strategy has great potential for reducing protein adsorption and cell attachment for a myriad of microfluidic applications.

RESULTS AND DISCUSSION

Two different microfluidic devices were designed to evaluate the antifouling behavior of the lipid bilayer coating. First, a rectangular cross-section microfluidic channel was used to characterize bilayer formation via bicelle-mediated rupture on solid supports and to determine the resistance of the lipid bilayer to nonspecific protein adsorption and cell attachment. Second, ten 5 μm constrictions designed to induce cellular deformation for intracellular delivery were utilized to examine fouling in constricted microfluidic devices (Figure 1A–C). The constriction dimensions were designed after previous reports that utilized squeezing for the delivery of biomacromolecules with increased accumulation of cell debris. These devices were fabricated using standard soft-lithographic strategies, binding a PDMS microfluidic channel to a clean glass substrate using plasma activation (Figure 1D). Bicelles were formed using a freeze-thaw-vortex cycle that was optimized by Kolahdouzan et al. and flowed into the microfluidic channel.[36] Lipid bicelles adsorb onto the channel walls and, upon reaching a critical surface concentration of adsorbed bicelles, rupture to form a conformal lipid bilayer coating through a process that is mediated by a combination of bicelle-substrate and bicelle-bicelle interactions. To characterize lipid bilayer formation in both devices, fluorescent bicelles were fabricated to have lipid compositions consisting of 1,2-dioleoyl-*sn*-glycero-3-phosphocholine (DOPC), 1,2-dihexanoyl-*sn*-glycero-3-phosphocholine (DHPC), and 1,2-dipalmitoyl-*sn*-glycero-3-phosphoethanolamine-*N*-(lissamine rhodamine B sulfonyl) (Rhod-PE). Lipid bilayer formation was observed in each microfluidic device, but the rate of its formation was found to differ based on channel geometry. Complete bilayer coverage in the rectangular microfluidic channel (Figure 2A,B) was observed after 45 min of bicelle exposure, whereas constricted microfluidic channels required longer exposure as described in the Materials and Methods section. These lipid bilayer coating protocols were applied to each microfluidic device for fouling and intracellular delivery experiments.

Fouling in microfluidics can occur when cells adhere to proteins that are secreted by the cell itself and adsorb to the channel wall. This protein-receptor interaction has been postulated as the primary mechanism for cell adhesion in polymer-based microfluidic devices.[37,38] To determine the protein resistance of our lipid coating, we analyzed the adsorption of fluorescein-isothiocyanate-labeled BSA (FITC-BSA) on our lipid-coated rectangular microfluidic channel (devices without constrictions). It has been reported that FITC-BSA can fill in defects in a lipid bilayer due to its strong affinity for silica supports and can be used as a metric for bilayer uniformity.[39] Initially, FITC-BSA was flowed into lipid bilayer-coated (bicelle) and bare (control) characterization devices, and protein adsorption was quantified by measuring the fluorescence intensity in the channel (Figure 2C). These measurements were normalized to the devices' background fluorescence, and each component of the microfluidic channel was also measured by separating the PDMS and glass with a razor blade. It was observed that lipid bilayer coatings resulted in >90%

Author Manuscript Author Manuscript Author Manuscript Author Manuscript

reduction in FITC-BSA adsorption on the assembled channel, the PDMS side walls, and the glass substrate (Figure 2D). This reduced protein adsorption confirmed a highly uniform lipid bilayer with few defects on all surfaces of the microfluidic device and led to evaluations of cell attachment using our bilayer coating.

Suspension (Jurkat) and adherent [human embryonic kidney (HEK)] cells were used to quantify cell attachment on both lipid bilayer-coated and bare microfluidic channels. The numbers of cells that attached to the channel walls were quantified using fluorescence microscopy. Jurkat cells were labeled with a live nuclear stain (Hoechst), and HEK cells were transfected to have fluorescently labeled mitochondria. Both cell types were flowed into microfluidic channels for 30 min with cell densities ranging from 10^5 to 10^7 cells/mL. Individual cells were quantified using ImageJ analysis software. It was observed that cell attachment increased with increasing cell density. However, lipid bilayer coatings resulted in >90% reductions in cell attachment for all cell densities tested and both cell types (Figure 2E–H). These reductions in nonspecific protein adsorption and cell fouling are comparable to levels achieved with gold-standard polymer coatings, such as poly(ethylene oxide)-coated surfaces.[38]

Given our observations of reduced cell attachment with a lipid layer, we applied our lipid bilayer coating strategy to constricted microfluidic devices. Note that the nonspecific adhesion of cells is a major issue for device performance and lifetime and is dependent on the geometry of the device.[40–42] For a device that is designed to have a squeezing dimension, the rate of cells that can be flowed through the constriction is limited. These constrictions result in objects that are larger than the squeezing dimension to clog and to disrupt flow through the device.[20] We investigated the ability of lipid bilayer coatings to reduce the accumulation of cell debris in our constricted microfluidic channels. Of note, the width of the channel was based on results from Han et al. who showed efficient intracellular delivery and high viability in 5 μm channel widths.[43] The length of the channel constriction (50 μm) was selected based on the results of Sharei et al. where a large amount of accumulated debris was observed in channels that had lengths larger than 30 μm.[5] The use of PDMS and glass materials with a hybrid of dimensions from Han et al. and Sharei et al. enabled a soft lithographic model system for analyzing the effectiveness of bicelle-mediated lipid bilayer coatings to reduce fouling in constricted microfluidic devices. After 25 million cells were flowed through lipid bilayer-coated and bare microfluidic constrictions, the cell debris was quantified using ImageJ software by measuring the area of the observable cellular debris and normalizing it to the device area, resulting in an average of 11% and 18% area of cell debris in lipid bilayer-coated and bare channels, respectively (Figure 3B). Evidence of cell debris in bilayer-coated constrictions led to additional evaluation of bilayer integrity after cell treatment using the fluorescent Rhod-PE bilayer composition. We observed reductions in fluorescence intensity at the microfluidic constriction outlet as a result of the bilayer being sheared away as cells pass through the constriction (Figure 3C). This decrease in fluorescence intensity in the sheared regions could be recovered by incubating the channel with a buffer for 6 h, which we attribute to lipid lability that results in lipid bilayer reorganization and recovery of defects, enabling further use or reuse of devices made in this way.

Author Manuscript Author Manuscript Author Manuscript Author Manuscript

To determine whether lipid bilayer-coated constrictions were effective for cell squeezing intracellular delivery, we tested the delivery of 40 kDa FITC-labeled dextran (FITC-Dex) to K562 3.21 and Jurkat cells, which are commonly used as lymphocyte models for gene-delivery applications. Fluorescence microscopy of K562 3.21 cells confirmed successful intracellular delivery of FITC-Dex showing bright fluorescence intensity as compared to the incubation control (Figure 4A,B). Jurkat cells incubated with FITC-Dex showed 13% fluorescent cells and were reported as the incubation control. Delivery of FITC-Dex using lipid bilayer-coated constrictions showed 57% and 65% delivery to K562 3.21 and Jurkat cells, respectively. We further investigated this platform's potential for plasmid delivery using an eGFP-expressing plasmid and observed 45% protein expression in Jurkat cells 48 h post-squeeze treatment (Figure 4C). Additionally, viabilities of FITC-Dex samples were observed to be 83% and 94% in K562 3.21 and Jurkat cells, respectively, whereas eGFP samples showed lower viability of 73% (Figure 4D). Note that there were no significant differences in delivery efficiency between Jurkat and K562 3.21 cells, despite differences in cell diameter (5 μm difference), and these results agree with observations from Sharei et al.[5] Flow cytometric analyses of successful intracellular delivery were applied with large shifts in fluorescence intensity for cells that were treated with constricted microfluidics (Figure 4E). Additional experiments using bare constricted channels showed no statistically significant differences in cell viability and delivery efficiency when compared to devices with lipid bilayer coatings (Figure S1). These results are comparable to efficiencies and viabilities observed in the previous cell squeezing work,[5,10] demonstrating that the lipid bilayer does not impede the formation of transient pores for intracellular delivery.

CONCLUSIONS AND PROSPECTS

Collectively, we have demonstrated a strategy to coat lipid bilayers onto glass and polymeric microfluidic supports using lipid bicelles. This lipid bicelle-mediated bilayer coating technique has demonstrated >90% reduction of protein adsorption and cell attachment, which we applied to constricted microfluidic channels that physically permeabilize cell membranes for intracellular delivery. Channels were designed to promote fouling with longer constriction lengths, and significant reductions in cell debris were observed in lipid bilayer-coated channels. Lipid bilayer-coated devices showed intracellular delivery performances that are comparable to those in previous reports, without fouling and clogging issues. We find three main advantages of using lipid bicelles in cell-squeezing microfluidics applications for intracellular delivery. First, using lipid bicelles offers a facile and versatile fabrication method for uniform lipid bilayer formation on standard microfluidic devices, requiring only freeze-thaw-vortex cycles and no special equipment. Second, the characterization of the devices can be easily made with standard fluorescence measurements, enabling direct observations of channel coating uniformity and integrity. Third, lipid bilayers formed through bicelle-mediated rupture show significant reductions in nonspecific protein adsorption and cell attachment in microfluidics that can be applied to cell applications beyond intracellular delivery. Future applications will explore improving the lipid bilayer rigidity similar to strategies that used air-stable supported lipid bilayers,[44] thereby preventing disruption of the lipid bilayer at the outlet of the microfluidic constrictions and reducing cell debris down to negligible amounts.

Author Manuscript Author Manuscript Author Manuscript Author Manuscript

MATERIALS AND METHODS

Bicelle Preparation Protocol.

All lipids including DOPC, DHPC, and 1,2-dipalmitoyl-*sn*-glycero-3-phos-phoethanolamine-*N*-(lissamine rhodamine B sulfonyl) were purchased from Avanti Polar Lipids. Small aliquots (1 mg) of DOPC and DHPC dissolved in chloroform were dried separately in test tubes under a gentle stream of nitrogen while being rotated to make a lipid film at the bottom of the tube and the dried lipid film was placed in a vacuum desiccator overnight. Next, the DOPC film was hydrated in an aqueous TRIS buffer (10 mM TRIS, 150 mM NaCl, pH 7.5) to a concentration of 63 μM to make a DOPC stock solution. The DOPC solution was subsequently used to hydrate the DHPC film to a final concentration of 252 μM, such that the molar ratio ("*q*-ratio") DOPC/DHPC is 0.25 between long- and short-chain lipids. The DOPC/DHPC mixture was transferred to a 50 mL falcon tube, and a small hole was punctured on the top using a syringe needle to alleviate pressure. The sample was plunged into liquid nitrogen for 1 min, followed by 5 min incubation in a 60 °C water bath (prepared on a hotplate prior to hydration) and vortexing for 30 s. This freeze-thaw-vortex cycle was repeated five times.

Microfluidic Device Fabrication.

Glass substrates were cleaned with piranha etch piranha solution is a 3:1 mixture of concentrated sulfuric acid with 30% hydrogen peroxide. It is a corrosive liquid and strong oxidizer. Proper safety precautions should be applied before use followed by sonication in Millipore deionized water (18.2 MΩ· cm) for 5 cycles of 5 min. The PDMS channels were fabricated with different dimensions, depending on the specific application. For fluidic devices designed to characterize lipid bilayer formation, straight channels were formed with a 2 mm × 27.5 mm × 0.05 mm silica mold that was fabricated using dry reactive etching. Constricted microfluidic channels for cell squeezing were designed to have a channel width of 25 μm that constricts to 5 μm for a 50 μm length and expands back to 25 μm with a total volume of 2 mm × 25 μm × 30 μm in the expanded regions. Inlets and outlets were formed using a 0.75 mm biopsy punch (Robbins) to make small holes in the PDMS. The PDMS channels and glass substrates were exposed to oxygen plasma (Harrick Plasma) for 90 s, at a power of 18 W with a chamber pressure of 10 psi, and were bound together immediately after being removed from the plasma chamber. The assembly was then placed in an oven set to 130 °C overnight. This plasma treatment and heating process enables a condensation reaction to occur between the plasma-activated glass and PDMS surfaces to form a covalent bond, sealing the microfluidic device. Polyethylene tubing (PE-50, Instech) was inserted into the inlet and outlet holes to form a tight seal.

Bilayer Formation.

Rectangular microfluidic channels were initially hydrated with TRIS buffer for 10 min using a syringe pump (Chemyx Fusion 3000) with a flow rate of 20 μL/min. Bicelles or fluorescently labeled bicelles (where the long-chain lipid consists of 99.5 mol % DOPC and 0.5 mol % 1,2-dipalmitoyl-*sn*-glycero-3-phos-phoethanolamine-*N*-(lissamine rhodamine B sulfonyl) lipid) were then flowed into the device with a flow rate of 20 μL/min for 30 min. In the constricted microfluidic channels, bilayer formation was significantly slower and

Author Manuscript Author Manuscript Author Manuscript Author Manuscript

required a flow rate of 5 μL/min for 12 h to ensure uniform coverage in the device. Lipid bilayer formation was confirmed using fluorescence microscopy (Axio Observer Z1, Zeiss). This process was followed by a washing step with a constant flow of TRIS buffer (20 μL/min) for another 30 min. Note that maintenance of channel hydration was carefully monitored using light microscopy after the addition of each solution, and all buffers and media were passed through a three-way valve (Harvard Apparatus) to force potential air bubbles away from the microfluidic channel before being introduced into the device. If air bubbles were observed to enter the channel, the bilayer would be damaged and the formation protocol would have to be repeated to ensure a uniform bilayer coating.

Protein Adsorption Protocol.

After washing the bilayer-coated channel with TRIS buffer, fluorescein isothiocyanate BSA (FITC-BSA, Sigma) was prepared in TRIS at a concentration of 0.3 mg/mL and was flowed through channels at 20 μL/min for 30 min. The channels were subsequently washed with TRIS using a flow rate of 50 μL/min for 30 min. Protein adsorption on the channel walls was determined using fluorescence microscopy and taking micrographs of the assembled channel and the PDMS and glass components after separating the two carefully with a razor blade. Relative fluorescence intensity of adsorbed FITC-BSA on each surface was quantified using ImageJ.

Cell Culture.

Jurkat cells (ATCC) and K562 3.21 cells generously provided by the Donald Kohn lab at UCLA were cultured in 1× RPMI 1640 with L-glutamine (Gibco) supplemented with 10% fetal bovine serum (Gibco) and 1% penicillin-streptomycin (10,000 units/mL penicillin and 10 mg/mL streptomycin) (Gibco). HEK cells (HEK 293T) were previously transfected to express fluorescent mitochondria as described previously[45] and were cultured using 1× Dulbecco's modified Eagle medium modified with D-glucose and L-glutamine (Gibco) supplemented with 10% fetal bovine serum and 1% penicillin-streptomycin.

Cell Adhesion and Clogging.

All buffers and cell culture media were filtered using 300 nm pore diameter syringe filters (Millipore) inside a laminar flow hood to prevent the introduction of dust. If the buffer or media was not used immediately, it was stored in the refrigerator at 4 °C and wrapped with parafilm until use. Cell culture media was also changed the day before each experiment. Jurkat cells and HEK cells with fluorescent mitochondria were provided by the Satiro De Oliveira and Michael Teitell labs at UCLA, respectively. Jurkat cell nuclei were labeled with Hoescht 33342 (Sigma) by adding 1 μL of 1 mg/mL Hoescht solution to Jurkat cells in 1 mL of cell culture media. The cell mixtures were incubated for 15 min at 37 °C and were used immediately for the following steps. Irrespective of the cell type, fluorescent cells suspended in a cell culture medium were collected via centrifugation at 500*g* for 5 min. The cell pellet was collected and dispersed in 1× phosphate-buffered saline solution (PBS, 137 mM NaCl, 2.7 mM KCl, 10 mM Na_2HPO_4, and 1.8 mM KH_2PO_4, Gibco) at a concentration of 1, 10, or 100 million cells/mL and passed through a 40 μm mesh cell strainer (Fisher) to reduce the number of cell aggregates (e.g., doublets, triplets). Cells were flowed into the characterization device using a syringe pump with a flow rate of 20 μL/min. Adhesion was

Author Manuscript Author Manuscript Author Manuscript Author Manuscript

quantified using fluorescence microscopy after washing with PBS buffer at 50 μL/min for 30 min. Cell adhesion was assessed by counting the cells that remained in the channel with ImageJ. For analyses of cell clogging in constricted microfluidic devices, Jurkat cells were dispersed in PBS buffer at 10 million cells/mL and flowed at 200 μL/min followed by a wash step at the same flow rate. Channel clogging was monitored by light microscopy and the area of cell debris remaining in the microfluidic device was quantified using ImageJ.

Intracellular Delivery.

Post-bilayer formation constricted microfluidic devices were prewashed with 1× PBS at a flow rate of 50 μL/min for 15 min. Cells were then dispersed at a density of 5 million cells/mL in a delivery medium consisting of 1% (v/v) Pluronic F-68 (Gibco) and 1× PBS, passed through a 40 μm mesh cell strainer, and collected into a 50 mL falcon tube (Thermo Fisher). Next, a final concentration of 0.1 mg/mL of eGFP-expressing plasmid (pCMV-GFP and Plasmid #11153, Addgene) or 0.3 mg/mL of 40 kDa FITC-labeled dextran (Invitrogen) was added to the delivery medium and collected into a 1 mL syringe. Cells were flowed through the microfluidic constrictions at 200 μL/min. An additional wash step of 1× PBS for 5 min followed and cells were incubated in the delivery medium for 10 min to facilitate membrane recovery and biomolecule diffusion. Cells were centrifuged at 500*g* for 5 min and dispersed in their respective culture media for further analyses. Viability was determined using a Cell Countess II (Invitrogen) and 0.4% trypan blue (Invitrogen).

Flow Cytometry.

Flow cytometry data were acquired and processed using an LSR Fortessa cytometer (BD Biosciences). Data analyses were performed using FlowJo software (FlowJo LLC). Fluorescence emission was stimulated using a 488 nm, 50 mW laser with a 505 nm long-pass filter and 515/20 nm bandpass filters for detecting green fluorescence. Delivery efficiency was reported as positive fluorescence from flow cytometry data. Positive fluorescence intensity was quantified using positive and negative controls and histograms were gated to identify the positive threshold intensity for a random 30,000 cell population from each sample.

Fluorescence Microscopy.

Cells were initially fixed via incubation in 0.5% paraformaldehyde (Sigma Aldrich) in 1× PBS solution. The cells were then spun down, dispersed in 1× PBS at a density of at least 1 million cells/mL, plated on microscope slides (Denville) in a 2:7 mixture of cells to ProLong diamond antifade mounting solution (Thermo Fisher), and mixed thoroughly using a P100 pipette (Gilson). A coverslip was carefully placed on top of the cell mixture and allowed to dry at room temperature for 1 h with foil covering the slides. Slides were stored at 4 °C and imaged within one week. Micrographs were recorded using an AxioZ1 Observer fluorescence microscope (Carl Zeiss AG) with EC Plan-Neofluar 2.5×/0.075, 10×/0.3, and LD Plan-Neofluor 20×/0.4, 40×/0.6 objectives. Fluorescence images were acquired using Zeiss filter sets (49 DAPI, 38 HE GFP, and 43 HE DsRed).

Author Manuscript Author Manuscript Author Manuscript Author Manuscript

Statistical and Image Analyses.

One-way ANOVA analyses were performed using Origin 9.1 data analysis and graphing software. Student's *t*-test was performed using GraphPad software. Quantification of cell adhesion utilized Fiji image analysis software.

Supplementary Material

Refer to Web version on PubMed Central for supplementary material.

ACKNOWLEDGMENTS

We thank Dr. John Abendroth, Dr. Kevin Cheung, Alexander Sercel, and Geoffrey Pronovost for helpful discussions on fluorescence and statistical analyses. We thank Prof. Zoran Galic (UCLA) and the UCLA Eli & Edythe Broad Center of Regenerative Medicine and Stem Cell Research for providing access to the Zeiss AxioZ1 Observer fluorescent microscope. We thank Profs. Satiro De Oliveira (UCLA), Donald Kohn (UCLA), and Mike Teitell (UCLA) for generously providing Jurkat, K562 3.21, and HEK cells, respectively. This work was supported by the National Institute on Drug Abuse (DA045550). J.N.B. thanks the NIH for a predoctoral fellowship; research reported in this publication was supported by the National Heart, Lung, and Blood Institute of the National Institutes of Health under Award Number F31HL149356. J.A.J. was supported by the National Research Foundation of Korea (NRF) grant funded by the Korean government (MSIT) (no. 2020R1C1C1004385). S.J.J. is supported by the NIH Common Fund through a NIH Director's Early Independence Award co-funded by the National Institute of Dental and Craniofacial Research and Office of the Director, NIH under award number DP5OD028181. S.J.J. also wishes to acknowledge Young Investigator Award funds from the Alex's Lemonade Stand Foundation for Childhood Cancer Research, the Hyundai Hope on Wheels Foundation for Pediatric Cancer Research, and the Tower Cancer Research Foundation. N.-J.C. was supported by a National Research Foundation Proof-of-Concept Grant (NRF2015NRF-POC001-019), and the Creative Materials Discovery Program through the National Research Foundation of Korea (NRF) that is funded by the Ministry of Science, ICT, and Future Planning (2016M3D1A1024098). P.S.W. and S.J.J. thank additional support and seed funding provided through a UCLA David Geffen School of Medicine Regenerative Medicine Theme Award. We acknowledge the facilities and thank the staff of the UCLA Eli & Edythe Broad Center of Regenerative Medicine and Stem Cell Research Flow Cytometry and Microscopy Core Facilities.

REFERENCES

(1). Stewart MP; Sharei A; Ding X; Sahay G; Langer R; Jensen KF In Vitro and ex Vivo Strategies for Intracellular Delivery. Nature 2016, 538, 183–192. [PubMed: 27734871]

(2). Carugo D; Ankrett DN; Glynne-Jones P; Capretto L; Boltryk RJ; Zhang X; Townsend PA; Hill M Contrast Agent-Free Sonoporation: The Use of an Ultrasonic Standing Wave Microfluidic System for the Delivery of Pharmaceutical Agents. Biomicrofluidics 2011, 5, 044108.

(3). Roth TL; Puig-Saus C; Yu R; Shifrut E; Carnevale J; Li PJ; Hiatt J; Saco J; Krystofinski P; Li H; Tobin V; Nguyen DN; Lee MR; Putnam AL; Ferris AL; Chen JW; Schickel J-N; Pellerin L; Carmody D; Alkorta-Aranburu G; Del Gaudio D; Matsumoto H; Morell M; Mao Y; Cho M; Quadros RM; Gurumurthy CB; Smith B; Haugwitz M; Hughes SH; Weissman JS; Schumann K; Esensten JH; May AP; Ashworth A; Kupfer GM; Greeley SAW; Bacchetta R; Meffre E; Roncarolo MG; Romberg N; Herold KC; Ribas A; Leonetti MD; Marson A Reprogramming Human T Cell Function and Specificity with Non-Viral Genome Targeting. Nature 2018, 559, 405–409. [PubMed: 29995861]

(4). Stewart MP; Langer R; Jensen KF Intracellular Delivery by Membrane Disruption: Mechanisms, Strategies, and Concepts. Chem. Rev 2018, 118, 7409–7531. [PubMed: 30052023]

(5). Sharei A; Zoldan J; Adamo A; Sim WY; Cho N; Jackson E; Mao S; Schneider S; Han M-J; Lytton-Jean A; Basto PA; Jhunjhunwala S; Lee J; Heller DA; Kang JW; Hartoularos GC; Kim K-S; Anderson DG; Langer R; Jensen KF A Vector-Free Microfluidic Platform for Intracellular Delivery. Proc. Natl. Acad. Sci. U.S.A 2013, 110, 2082–2087. [PubMed: 23341631]

(6). Ding X; Stewart MP; Sharei A; Weaver JC; Langer RS; Jensen KF High-Throughput Nuclear Delivery and Rapid Expression of DNA via Mechanical and Electrical Cell-Membrane Disruption. Nat. Biomed. Eng 2017, 1, 0039. [PubMed: 28932622]

Author Manuscript Author Manuscript Author Manuscript Author Manuscript

(7). Liu Z; Han X; Zhou Q; Chen R; Fruge S; Jo MC; Ma Y; Li Z; Yokoi K; Qin L Integrated Microfluidic System for Gene Silencing and Cell Migration. Adv. Biosyst 2017, 1, 1700054. [PubMed: 28890929]

(8). Liu A; Islam M; Stone N; Varadarajan V; Jeong J; Bowie S; Qiu P; Waller EK; Alexeev A; Sulchek T Microfluidic Generation of Transient Cell Volume Exchange for Convectively Driven Intracellular Delivery of Large Macromolecules. Mater. Today 2018, 21, 703–712.

(9). Carugo D; Ankrett DN; Glynne-Jones P; Capretto L; Boltryk RJ; Zhang X; Townsend PA; Hill M Contrast Agent-Free Sonoporation: The Use of an Ultrasonic Standing Wave Microfluidic System for the Delivery of Pharmaceutical Agents. Biomicrofluidics 2011, 5, 044108.

(10). Liu C; Zhang W; Li Y; Chang J; Tian F; Zhao F; Ma Y; Sun J Microfluidic Sonoporation to Assemble Exosome Membrane-Coated Nanoparticles for Immune Evasion-Mediated Targeting. Nano Lett. 2019, 19, 7836–7844. [PubMed: 31597431]

(11). Belling JN; Heidenreich LK; Tian Z; Mendoza AM; Chiou T-T; Gong Y; Chen NY; Young TD; Wattanatorn N; Park JH; Scarabelli L; Chiang N; Takahashi J; Young SG; Stieg AZ; De Oliveira S; Huang TJ; Weiss PS; Jonas SJ Acoustofluidic Sonoporation for Gene Delivery to Human Hematopoietic Stem and Progenitor Cells. Proc. Natl. Acad. Sci. U.S.A 2020, 117, 10976. [PubMed: 32358194]

(12). Kang G; Carlson DW; Kang TH; Lee S; Haward SJ; Choi I; Shen AQ; Chung AJ Intracellular Nanomaterial Delivery via Spiral Hydroporation. ACS Nano 2020, 14, 3048–3058. [PubMed: 32069037]

(13). Sharei A; Poceviciute R; Jackson EL; Cho N; Mao S; Hartoularos GC; Jang DY; Jhunjhunwala S; Eyerman A; Schoettle T; Langer R; Jensen KF Plasma Membrane Recovery Kinetics of a Microfluidic Intracellular Delivery Platform. Integr. Biol 2014, 6, 470–475.

(14). Ma Y; Han X; Quintana Bustamante O; Bessa De Castro R; Zhang K; Zhang P; Li Y; Liu Z; Liu X; Ferrari M; Hu Z; Carlos Segovia J; Qin L Highly Efficient Genome Editing of Human Hematopoietic Stem Cells via a Nano-Silicon-Blade Delivery Approach. Integr. Biol 2017, 9, 548–554.

(15). DiTommaso T; Cole JM; Cassereau L; Buggé JA; Hanson JLS; Bridgen DT; Stokes BD; Loughhead SM; Beutel BA; Gilbert JB; Nussbaum K; Sorrentino A; Toggweiler J; Schmidt T; Gyuelveszi G; Bernstein H; Sharei A Cell Engineering with Microfluidic Squeezing Preserves Functionality of Primary Immune Cells in Vivo. Proc. Natl. Acad. Sci. U.S.A 2018, 115, E10907–E10914. [PubMed: 30381459]

(16). Yuan W-M; Shao J-Y; Xue C-D; Liu B; Qin K-R A High-Throughput Microfluidic Device for Probing Calcium Dynamics of Single Cells Squeezing through Narrow Channels. J. Micromech. Microeng 2019, 29, 115014.

(17). Ocvirk G; Munroe M; Tang T; Oleschuk R; Westra K; Harrison D-J Electrokinetic Control of Fluid Flow in Native Poly(dimethylsiloxane) Capillary Electrophoresis Devices. Electrophoresis 2000, 21, 107. [PubMed: 10634476]

(18). Wu M-H Simple Poly(dimethylsiloxane) Surface Modification to Control Cell Adhesion. Surf. Interface Anal 2009, 41, 11–16.

(19). Boxshall K; Wu M-H; Cui Z; Cui Z; Watts JF; Baker MA Simple Surface Treatments to Modify Protein Adsorption and Cell Attachment Properties within a Poly(dimethylsiloxane) Micro-Bioreactor. Surf. Interface Anal 2006, 38, 198–201.

(20). Lee W; Tseng P; Di Carlo D Microfluidic Cell Sorting and Separation Technology. In Microtechnology for Cell Manipulation and Sorting; Lee W, Tseng P, Di Carlo D, Eds.; Springer: Cham, 2017; pp 1–14.

(21). Kim P; Jeong HE; Khademhosseini A; Suh KY Fabrication of Non-Biofouling Polyethylene Glycol Micro- and Nanochannels by Ultraviolet-Assisted Irreversible Sealing. Lab Chip 2006, 6, 1432–1437. [PubMed: 17066166]

(22). Mukhopadhyay R When Microfluidic Devices Go Bad. Anal. Chem 2005, 77, 429A–432A.

(23). Sut TN; Jackman JA; Cho NJ Understanding How Membrane Surface Charge Influences Lipid Bicelle Adsorption onto Oxide Surfaces. Langmuir 2019, 35, 8436–8444. [PubMed: 31141663]

Author Manuscript Author Manuscript Author Manuscript Author Manuscript

(24). Sut TN; Jackman JA; Yoon BK; Park S; Kolahdouzan K; Ma GJ; Zhdanov VP; Cho N-J Influence of NaCl Concentration on Bicelle-Mediated SLB Formation. Langmuir 2019, 35, 10658–10666. [PubMed: 31318563]

(25). Belling JN; Cheung KM; Jackman JA; Sut TN; Allen M; Park JH; Jonas SJ; Cho N-J; Weiss PS Lipid Bicelle Micropatterning Using Chemical Lift-Off Lithography. ACS Appl. Mater. Interfaces 2020, 12, 13447–13455. [PubMed: 32092250]

(26). Jackman JA; Cho N-J Supported Lipid Bilayer Formation: Beyond Vesicle Fusion. Langmuir 2020, 36, 1387–1400.

(27). Yang T; Jung S.-y.; Mao H; Cremer PS Fabrication of Phospholipid Bilayer-Coated Microchannels for On-Chip Immuno-assays. Anal. Chem 2001, 73, 165–169. [PubMed: 11199961]

(28). Makamba H; Kim JH; Lim K; Park N; Hahn JH Surface Modification of Poly(dimethylsiloxane) Microchannels. Electrophoresis 2003, 24, 3607–3619. [PubMed: 14613185]

(29). Chiu DT; Jeon NL; Huang S; Kane RS; Wargo CJ; Choi IS; Ingber DE; Whitesides GM Patterned Deposition of Cells and Proteins onto Surfaces by Using Three-Dimensional Microfluidic Systems. Proc. Natl. Acad. Sci. U.S.A 2000, 97, 2408–2413. [PubMed: 10681460]

(30). Groves JT; Dustin ML Supported Planar Bilayers in Studies on Immune Cell Adhesion and Communication. J. Immunol. Methods 2003, 278, 19–32. [PubMed: 12957393]

(31). Huang C-J; Cho N-J; Hsu C-J; Tseng P-Y; Frank CW; Chang Y-C Type I Collagen-Functionalized Supported Lipid Bilayer as a Cell Culture Platform. Biomacromolecules 2010, 11, 1231–1240. [PubMed: 20361729]

(32). Vafaei S; Tabaei SR; Biswas KH; Groves JT; Cho N-J Dynamic Cellular Interactions with Extracellular Matrix Triggered by Biomechanical Tuning of Low-Rigidity, Supported Lipid Membranes. Adv. Healthcare Mater 2017, 6, 1700243.

(33). Persson F; Fritzsche J; Mir KU; Modesti M; Westerlund F; Tegenfeldt JO Lipid-Based Passivation in Nanofluidics. Nano Lett. 2012, 12, 2260–2265. [PubMed: 22432814]

(34). Groves JT; Mahal LK; Bertozzi CR Control of Cell Adhesion and Growth with Micropatterned Supported Lipid Membranes. Langmuir 2001, 17, 5129–5133.

(35). Andersson A-S; Glasmästar K; Sutherland D; Lidberg U; Kasemo B Cell Adhesion on Supported Lipid Bilayers. J. Biomed. Mater. Res., Part A 2003, 64, 622–629.

(36). Kolahdouzan K; Jackman JA; Yoon BK; Kim MC; Johal MS; Cho N-J Optimizing the Formation of Supported Lipid Bilayers from Bicellar Mixtures. Langmuir 2017, 33, 5052–5064. [PubMed: 28457139]

(37). Chen CS; Mrksich M; Huang S; Whitesides GM; Ingber DE Geometric Control of Cell Life and Death. Science 1997, 276, 1425–1428. [PubMed: 9162012]

(38). Liu VA; Jastromb WE; Bhatia SN Engineering Protein and Cell Adhesivity Using PEO-Terminated Triblock Polymers. J. Biomed. Mater. Res 2002, 60, 126–134. [PubMed: 11835168]

(39). Glasmästar K; Larsson C; Höök F; Kasemo B Protein Adsorption on Supported Phospholipid Bilayers. J. Colloid Interface Sci 2002, 246, 40–47. [PubMed: 16290382]

(40). Dressaire E; Sauret A Clogging of Microfluidic Systems. Soft Matter 2017, 13, 37–48.

(41). Hou X; Zhang YS; Santiago GT; Alvarez MM; Ribas J; Jonas SJ; Weiss PS; Andrews AM; Aizenberg J; Khademhosseini A Interplay between Materials and Microfluidics. Nat. Rev. Mater 2017, 2, 17016.

(42). Green JV; Kniazeva T; Abedi M; Sokhey DS; Taslim ME; Murthy SK Effect of Channel Geometry on Cell Adhesion in Microfluidic Devices. Lab Chip 2009, 9, 677–685. [PubMed: 19224017]

(43). Han X; Liu Z; Jo MC; Zhang K; Li Y; Zeng Z; Li N; Zu Y; Qin L CRISPR-Cas9 Delivery to Hard-to-Transfect Cells via Membrane Deformation. Sci. Adv 2015, 1, e1500454. [PubMed: 26601238]

(44). Deng Y; Wang Y; Holtz B; Li J; Traaseth N; Veglia G; Stottrup BJ; Elde R; Pei D; Guo A; Zhu XY Fluidic and Air-Stable Supported Lipid Bilayer and Cell-Mimicking Microarrays. J. Am. Chem. Soc 2008, 130, 6267–6271. [PubMed: 18407640]

Author Manuscript Author Manuscript Author Manuscript Author Manuscript

(45). Miyata N; Steffen J; Johnson ME; Fargue S; Danpure CJ; Koehler CM Pharmacologic Rescue of an Enzyme-Trafficking Defect in Primary Hyperoxaluria 1. Proc. Natl. Acad. Sci. U.S.A 2014, 111, 14406–14411. [PubMed: 25237136]

Author Manuscript Author Manuscript Author Manuscript Author Manuscript

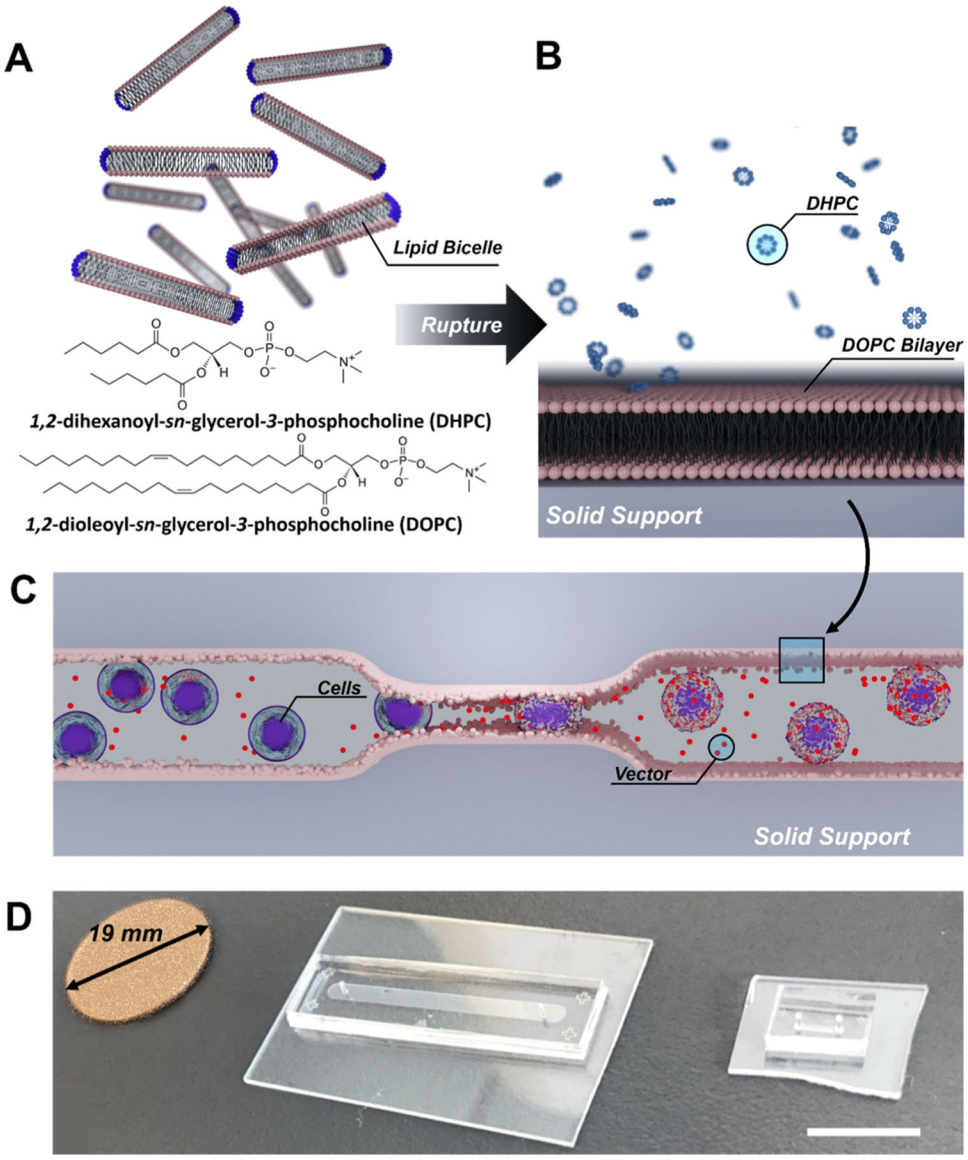

Figure 1.

Schematic of bilayer formation and lipid bilayer microfluidic devices. (A) Schematic of lipid bicelles consisting of long- (DOPC) and short-chain (DHPC) phospholipids. (B) Schematic of bicelles rupturing on a solid support to form a supported lipid bilayer, resulting in DHPC monomers and micelles released into the surrounding aqueous solution. (C) Schematic of a supported lipid bilayer coating a cell-squeezing device and depiction of cell squeezing. As cells pass through the microfluidic constriction, the cells deform, causing transient pore formation and the delivery of biomolecular cargo (red) via diffusion. (D) Images of the characterization device and lipid-coated squeezing device (coin for scale). Scale bar is 15 mm.

Author Manuscript Author Manuscript Author Manuscript Author Manuscript

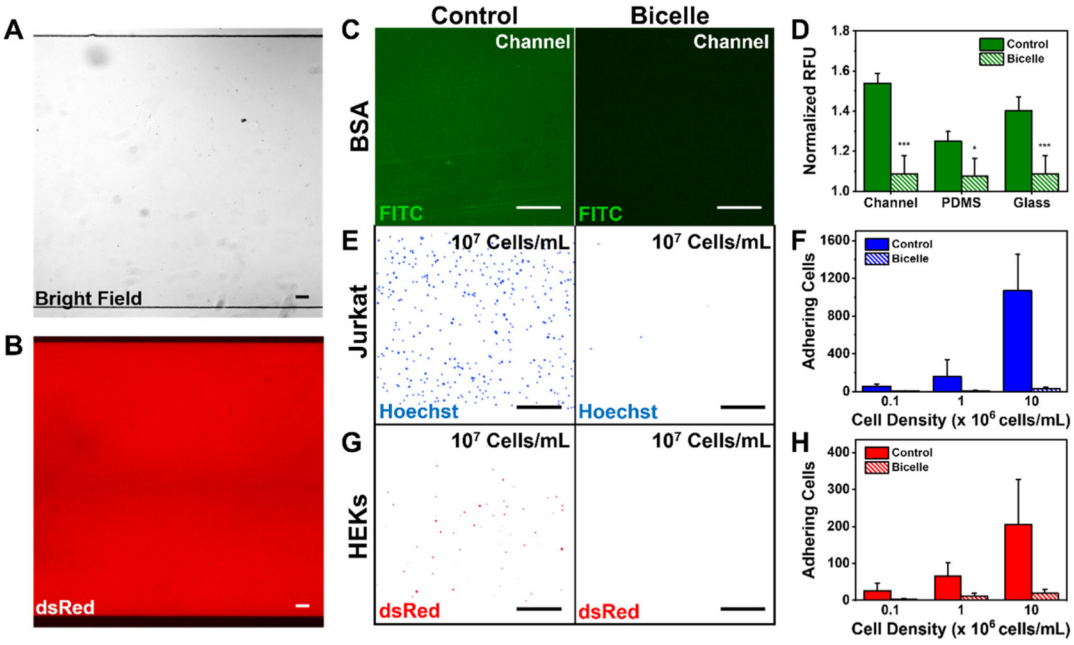

Figure 2.

Analyses of protein adsorption and cell adhesion in lipid-coated and bare channels. (A) Brightfield image and (B) fluorescent micrograph of the microfluidic channel after the introduction of fluorescently labeled lipid bicelles. (C) Fluorescent micrographs of bare (control) and bilayer-coated (bicelle) microfluidic channels after the introduction of FITC (green)-labeled BSA (FITC-BSA). (D) Normalized relative fluorescence intensity of adsorbed FITC-BSA for each component of the microfluidic characterization device including the fully assembled channel (channel), the PDMS, and the glass substrate (glass) for bicelle and control samples. (E) Fluorescent micrographs after 10^7 suspension (Jurkat) cells/mL were flowed through the control and bicelle channels. (F) Number of adhered Jurkat cells as a function of initial cell density. (G) Fluorescent micrographs after 10^7 adherent HEK cells were flowed in the control and bicelle channels. (H) Number of adhered HEKs as a function of initial cell density. Jurkat cell nuclei were stained with Hoechst (blue) before the cells were flowed into the channels. The HEKs were previously transfected to have fluorescently labeled mitochondria (dsRed, red). Panels (E,F) were inverted and false-colored to match emitted fluorescence for clarity. The data represent $N = 4$ trials with standard deviations for error bars. Statistics were derived using a one-way ANOVA (Origin) and Tukey's test.

Author Manuscript Author Manuscript Author Manuscript Author Manuscript

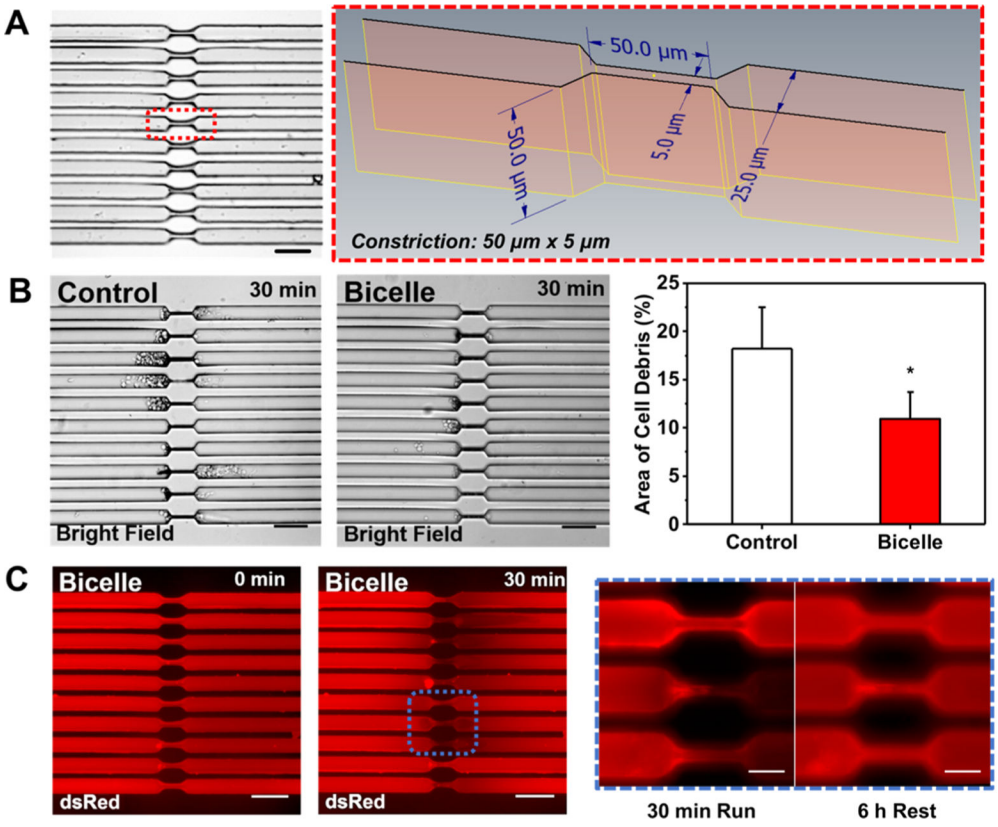

Figure 3.

Characterization of cell debris in lipid-coated channels. (A) Image of the constricted microfluidic channel pre-cell treatment. (Red-dash Inset) Schematic of the microfluidic constriction dimensions. (B) Images of the cell-squeezing device post-cell treatment for bilayer-coated (bicelle) and bare (control) constricted channels. The percentages of adhered Jurkat cells and cell debris normalized to the device area after 25 million cells were flowed through bicelle and control microfluidic channels. Cell debris was quantified by measuring the observable area of cellular debris accumulation. The value was normalized to the total device area and reported as a percentage. (C) Fluorescent micrographs of fluorescently labeled bilayer-coated cell squeezing channels (bicelle, dsRed) pre-cell treatment (0 min) and post-cell treatment (30 min). (Blue-dash Inset) High magnification (40×) fluorescent micrographs of the lipid bilayer-coated microfluidic constriction post-cell treatment and a buffer wash step (30 min Run) and 6 h after incubating the channel in PBS (6 h Rest). The data represents $N = 4$ trials with standard deviations for error bars. Statistics were derived using Student's t-test, and scale bars are 50 μm.

Author Manuscript Author Manuscript Author Manuscript Author Manuscript

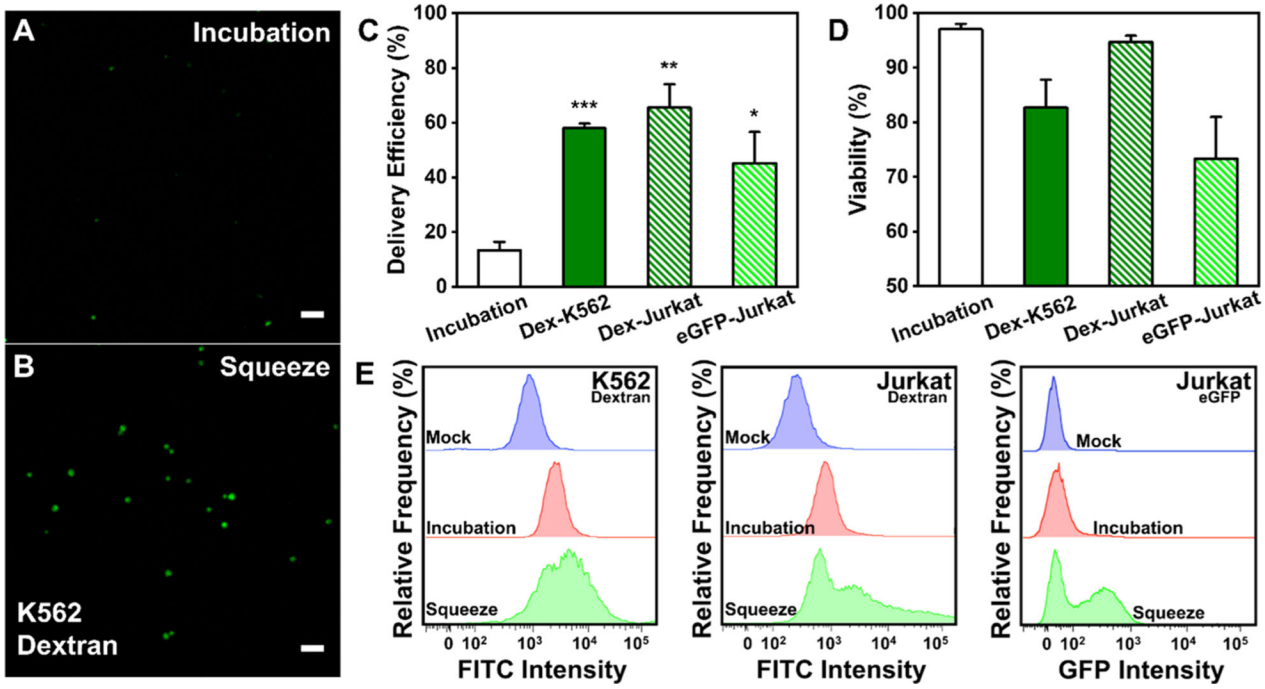

Figure 4.

Transfection efficiency and viability of lipid bilayer-coated channels. (A) Confocal laser scanning micrograph of cells incubated with FITC-labeled 40 kDa dextran (FITC-Dex, green) and (B) K562 3.21 cells post-cell squeezing. (C) Delivery efficiency of FITC-Dex and eGFP using bicelle-coated cell-squeezing devices with K562 3.21 and Jurkat cells. Dextran samples were measured 30 min post-cell squeezing, whereas eGFP samples were measured 48 h later. (D) Cell viability at 30 min and 48 h post-cell squeezing of K562 3.21 and Jurkat cells using FITC-Dex and eGFP, respectively, as the biomolecular cargo. (E) Representative flow cytometry histograms for untreated cells (mock) or K562 3.21 and Jurkat cells that were incubated or squeezed with FITC-Dex or eGFP in the delivery medium. The data represents $N = 4$ trials with standard deviations for error bars. Statistics were done using a one-way ANOVA (Origin), and Tukey's test and scale bars are 50 μm.